# MODELLING OF WIND TURBINE BLADE TRAILING EDGE CORE DESIGNED AND OPTIMIZED FOR RAPID PROTOTYPING

Aske H. Petersen, Dennis M. Pedersen, Jes M. Jensen, Kristian Jakobsen, Riccardo Grosselle

Department of Materials and Production, Aalborg University
Fibigerstraede 16, DK-9220 Aalborg East, Denmark
Email: {apete18, dpeder18, jmje18, kjakob18, rgross21}@student.aau.dk,
Web page: http://www.mechman.mp.aau.dk/

**Abstract**

This paper describes a method for rapid prototyping of a trailing edge core, used by Siemens Gamesa Renewable Energy, while not compromising the structural integrity of the wind turbine blade. Different additive manufacturing methods for rapid prototyping and a selection of suitable materials are presented. Moreover, a model is built in Ansys Composite Prep-Post to evaluate the structural performance in buckling, strength and in-plane stiffnesses of the trailing edge. The analyses are based on a "*Student Blade*" 112 [m] wind turbine blade model, supplied by SGRE with appropriate lay-ups, boundary conditions and loads.

**Keywords:** Composite design and analysis, Finite element analysis, Numerical optimization, Wind turbine blade, Trailing Edge

## 1. Introduction

The world is increasingly transitioning towards a greener and more sustainable energy production to reach environmental goals, and as such a need for optimizing current technologies is necessary. Siemens Gamesa Renewable Energy (SGRE) is among the market leaders within the wind industry, as designers and manufacturers of wind turbines. As they look to produce affordable energy by optimizing both the power generated from the turbines, but also manufacturing processes, they have developed a patented method of manufacturing blades called IntegralBlade®, where each blade is cast in one piece. This eliminates the glued joints at the leading edge (LE) and trailing edge (TE), which are normally needed in wind turbine blades. With IntegralBlade®, new production methods have been employed leading to new structural challenges both during casting and operation. Specifically, a core is introduced in the TE to ensure manufacturing capabilities, as the vacuum bags, used in casting production, might incur the risk of rupturing/puncturing as the cross-section becomes thinner towards the TE. Due to this limit, additional core material is needed to separate the top and bottom face sheets at the TE [1].

Figure 1 illustrates a generalized cross-section of a wind turbine with a single shear web and no glued joints. The LE is the edge facing towards the direction of rotation, and in principle "splitting" the air into the pressure side (PS) and the suction side (SS). Figure 2 shows a zoomed view of the TE and its reinforcement, known as the TE core. The current core is made of foamed polyurethane (PUR), which is cast in 1.2 [m] segments to improve handling during production.

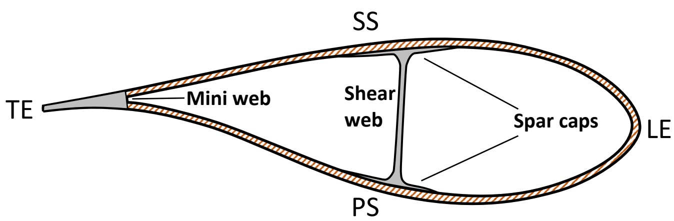


*Fig. 1 Generalized cross-section of a wind turbine blade. [1]*

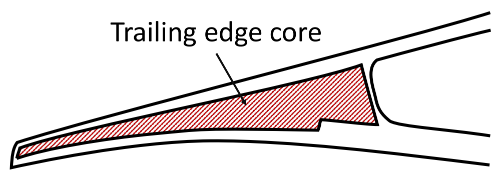


*Fig. 2 Zoomed view of the TE core used in production at SGRE.*

The four main loading directions are leading-to-trailing (LTT), pressure-to-suction (PTS) and the reverse (TTL & STP). The load cases which exert the largest load on the TE core are the LTT and TTL.

Due to the location of the TE core, it contributes significantly to the buckling resistance of the blade when loaded in LTT. This is revealed by a preliminary buckling analysis of the Student Blade, which is a simplified finite element (FE) model of the 112 [m] blade, where the composite lay-ups and load scenarios are implemented. The outer geometry is constituted by SHELL181 elements, whereas the TE core is modelled with SOLID187 elements. From the analysis, the load multiplier is calculated to be a factor of three higher with the TE core, compared to without any TE core present.

The purpose of this paper is to present a solution for rapid prototyping of the TE core, without compromising the structural integrity. In the following, the current manufacturing method and suitable additive manufacturing methods are presented and modelled. Additionally, the structural integrity of the proposed solution is evaluated in regard to the essential properties; buckling, in-plane cross-sectional stiffnesses and strength.

## 2. Manufacturing of the TE core

The TE core is made by reaction injection moulding of PUR as described in [2]. Utilizing this method, strict tolerances of density, mechanical properties, and dimensions of the foam can be kept, by controlling the flow rate, temperature and pressure.

For every TE core section, a unique mould is constructed. As these sections are small in comparison to the entire length of the blade, multiple moulds must be produced, which results in a lead time for the TE core of up to six months, according to SGRE. As a result, producing the moulds is one of the earliest stages in the blade manufacturing process, thus limiting the possibility to modify or change the design and manufacturing process of the blade.

Due to the current lead time for the production of moulds, it would be beneficial to investigate the possibilities of reducing the lead time by using a manufacturing method capable of rapid prototyping, ultimately leading to more freedom in the design process.

### 2.1 Additive manufacturing

Based on [3] and [4] three general additive manufacturing methods are presented for rapid prototyping; stereolithography (SLA), selective laser sintering (SLS) and fused deposition modelling (FDM).

#### *2.1.1 Stereolithography*

SLA is based on the principle that an object is shaped layer-by-layer using ultraviolet light aimed at a liquid photopolymer resin inside a vat. Each layer is formed by hardening the resin with the light source. After completion, the remaining resin is drained from the vat, and the model is removed, washed and in some cases post cured, due to internal volumes filled with resin.

The key advantage of using SLA is that it is fast and it yields a better surface finish compared to other additive manufacturing methods, as it can achieve tolerances down to 0.0125 [mm].

The key disadvantage of using SLA is that there is a limited number of materials available suitable for manufacturing, most of which cannot be used for temperatures above 50 $[°C]$. Moreover, it is relatively expensive compared to other additive manufacturing processes.

#### *2.1.2 Selective laser sintering*

SLS is the manufacturing of components by using a laser that melts and sinters a powdered semicrystalline polymer or metal. To create each layer, a roller deposits a thin layer of powder onto a platform, followed by a laser, sintering a specific cross-section of a model.

The key advantage of SLS is that a wider selection of materials, such as polymers, thermoplastic elastomers and metals are available. Additionally, the sintered part has a high resistance to elevated temperatures.

Disadvantage of SLS includes that it has a more coarse surface finish compared to SLA. Internal stresses can appear, leading to warping of the parts and similarly to SLA, it might produce internal volumes filled with material. However, unlike SLA, SLS cannot be post-cured, and to mitigate this, drain holes are necessary if hollow walls or internal voids are produced.

#### *2.1.3 Fused deposition modelling*

FDM is commonly known as ”3D printing” and is used to produce complex parts out of primarily thermoplastic polymer filament. This is heated and fed through an extruder that deposits the melted polymer on previous layers forming a single layer of the entire component. In Figure 3 the process of FDM is illustrated.

A key disadvantage of FDM is the weak adhesion between subsequent layers, increasing the risk of delamination under complex load cases. This also indicates that the material properties of FDM parts are highly orientation dependent. Lastly, as the material is added to previous layers, the method is incapable of producing large overhangs. As FDM generally has the largest possible build volume, lowest price and flow rate of the technologies presented, it is seen as a suitable

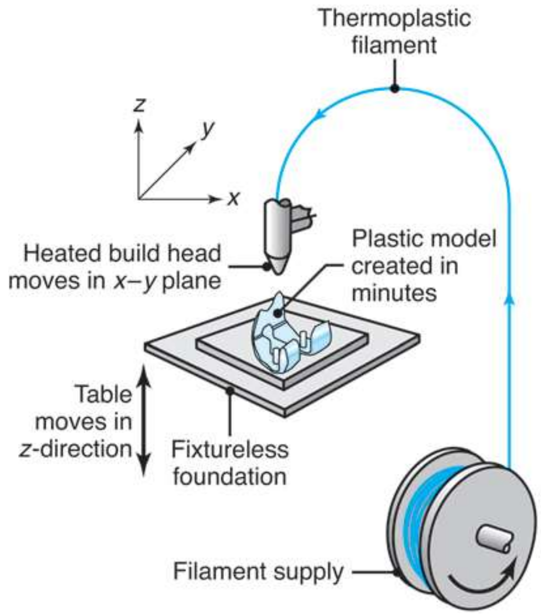


*Fig. 3 Illustration of FDM manufacturing process [3].*

manufacturing method for rapid prototyping of the TE core.

The evaluation is based on the SLA machine *"ProX 950"* [5], SLS machine *"Sindoh S100"* [6] and FDM machine *"BLB Industries The BOX SMALL"* [7]. These machines are taken as representative of industry capable machines. However, as the technology develops rapidly all parameters for each machine are expected to improve, especially the price pr. machine.

### *2.1.4 Material selection*

A large number of FDM filaments are available on the market, even the most common FDM filaments exist in a multitude of different variants, each with different properties. Based on [8] a material selection is done, where polycarbonate (PC) is chosen as the most suitable material for rapid prototyping of the TE core. PC generally shows the greatest compromise between density, stiffness and cost. Furthermore, it has a service temperature similar to PUR. However, as the density is larger by a factor of approximately 8 than that of the original material, it is necessary to reduce the mass of the TE core, if the overall mass of the blade is to be kept to a minimum.

### *2.1.5 Material modelling*

When 3D printing a component with FDM, the structure and shape inside, commonly referred to as *infill*, are often different and can assume various complex forms. This detail is one of the reasons why 3D printing is becoming increasingly popular within the rapid prototyping world, as it allows to speed up the process, and save material, while still maintaining the outer shape of the component as designed.

However, infill poses a challenge for the engineer, in case the 3D printed component is to be verified through the use of FE analysis, as the material properties are difficult to obtain, either numerically or experimentally.

A more direct and rapid approach is presented in [9], according to which the elastic properties of 3D printed parts are simulated by using the "Material Designer" plug-in within Ansys.

According to [10], the Material Designer allows to calculate the properties of a homogenized material using the known properties of its constituents.

In practice, this means that instead of simulating the full microstructure, the mechanical properties are averaged. The starting point for the analysis is the Representative Volume Element (RVE) which is defined as the smallest possible unit, which includes enough constituents to represent the properties of the entire microstructure in a statistically representative manner [11].

In order to find the homogenized material properties, as described in [10], the RVE is subjected to a total of six load cases; three tensile tests (x-, y- and z-direction) and three shear tests (xy, yz and xz). Here the RVE is subjected to a macroscopic strain of $\varepsilon = 0.001$ [mm/mm].

## 3. Structural analyses

A preliminary analysis of the existing structure is performed to characterise the stiffness and buckling behaviour as a baseline for the evaluation of optimized solutions. The analyses are done using both the Student Blade FE model and a more detailed solid model built in Ansys Composite Prep-Post (ACP).

Offset is taken from a cross-section at 80 [m], which is extruded 3 [m] to form a sub-model segment. This utilizes the assumption that the cross-section remains constant through the length of 3 [m], thus neglecting the double curvature.

Although this assumption is inherently wrong, it is assumed sufficient, as the cross-section generally remains similar in shape and size in this segment of the blade.

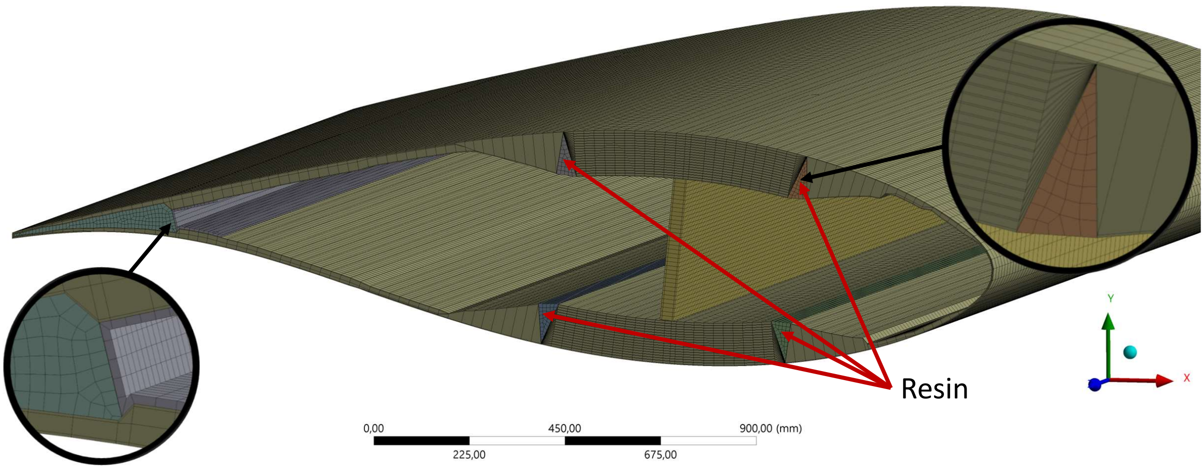


*Fig. 4 Full 3 [m] sub-model with MPC connections and resin filled voids indicated.*

### 3.1 Modelling

ACP is used to model the composite lay-up in Ansys. The pre-processing mode maps the composite definitions to a given shell geometry, which can be integrated into Ansys Workbench as a solid composite model, and used in detailed analyses. Combining the information supplied from SGRE the 3 [m] sub-model can be seen in Figure 4, which has a chord length of approximately 2.4 [m] and a height of 0.55 [m].

The model consists of 5 primary parts; *outer shell*, *shear web*, *mini web*, *TE core* and *resin filled voids*, each modelled separately and combined using multi-point constraint (MPC) based contacts. The latter, *resin-filled voids*, is used in the discrepancy between the drop-off from the spar caps to the outer shell.

#### *3.1.1 Element types*

The element used in the 3 [m] sub-model is SOLID185, which is an 8-node hexahedral element, with the ”enhanced strain formulation” enabled to prevent shear locking in bending problems. The element has three degrees of freedom per node, i.e. translation in the x-, y- and z-direction.

The mesh is seen in Figure 4. The resin-filled voids are highlighted together with the side web and adjacent connections. The outer shell is modelled with an element size of 25 [mm] in width, whereas the height of each layer is modelled with one element in thickness, with the element height adapting to the layer thickness.

The mini web, shear web, TE core and resin-filled voids use an element size of 10 [mm]. In total, the 3 [m] sub-model consists of 639007 nodes and 410317 elements.

### 3.2 Buckling

Buckling is used to assess the out-of-plane behaviour of the 3 [m] sub-model. As mentioned in [12], buckling occurs at the loss of stability of an equilibrium configuration. Both a linear eigenvalue buckling and non-linear buckling analysis are performed, where the linear analysis works as a preliminary evaluation of the behaviour and as a starting point for the non-linear analysis. The general incremental equilibrium equation, in FE form, used in non-linear buckling analysis is seen in Equation (1).

$$([K_0] + [K_L(\{D\})] + [K_\sigma])\{\Delta D\} = -\{R\} \qquad (1)$$

Here $[K_0]$ is the linear stiffness matrix, $[K_L]$ is the *initial* displacement stiffness matrix, i.e. it is updated to take the deformed geometry for each load step into account. $[K_\sigma]$ accounts for stiffness due to membrane forces, $\{\Delta D\}$ is the incremental displacement relative to the reference configuration and $\{R\}$ is residual force.

Similarly, the linear eigenvalue buckling can be written as an incremental equilibrium equation, as seen in Equation (2) and is solved as an eigenvalue problem.

Here the difference between the non-linear equation is that $[K_L]$ is not present, as the deformed geometry is not taken into account, i.e. the reference geometry is used. For the same reasons $[K_\sigma]$ scales linearly, and furthermore, the external forces are neglected as the solution takes offset in an equilibrium equation between two deformation paths at the same load.

$$([K_0] + \lambda[K_\sigma])\{\delta D\} = \{0\} \qquad (2)$$

An illustration of the Ansys setup is seen in Figure 5, with displacements supports A and B at the ends of the shear web having all translational degrees of freedom

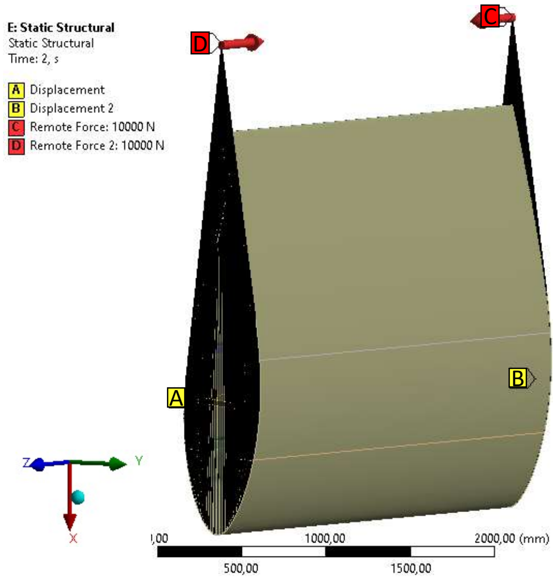


*Fig. 5 Setup of the buckling analysis in Ansys Workbench.*

locked. Additionally, the forces of 10 [kN], which are chosen arbitrarily, are applied at remote points (C and D) above the structure, based on the setup from [13]. Utilizing this setup and boundary conditions, the 3 [m] sub-model is loaded in 2-point bending and buckling is assessed.

The non-linear buckling analysis utilizes a similar setup; although the forces are increased to 1.8 [MN], which is equal to the load multiplier of the first mode of the linear eigenvalue buckling ($\lambda_1 = 181.19$) multiplied with the force of 10 [kN]. Additionally, the force is applied in multiple load steps to accurately capture the 'load-deflection' behaviour.

### 3.3 In-plane stiffnesses

The in-plane stiffnesses are characterized using a simplified model of the 3 [m] sub-model, where a section cut is made at the transition zone from the outer shell to spar caps. Moreover, the 3 [m] sub-model is reduced to 100 [mm] instead, thereby imitating an in-plane situation. The setup is shown in Figure 6, where points A and B are excited with a unit displacement separately.

Each point is limited to three degrees of freedom, i.e. translation in x- and y-direction and rotation (positive counter-clockwise) around the z-axis.

With the general form, the stiffness matrix can be expressed as seen in Equation (3).

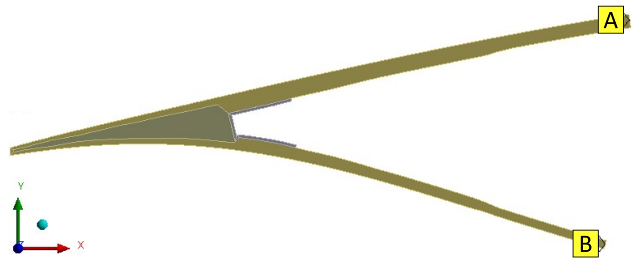


*Fig. 6 Model and setup used for in-plane stiffness analysis, with a solid composite model.*

$$\underbrace{\begin{Bmatrix} F_{Ax} \\ F_{Ay} \\ M_{Az} \\ F_{Bx} \\ F_{By} \\ M_{Bz} \end{Bmatrix}}_{\{R\}} = \underbrace{\begin{bmatrix} K_{11} & K_{12} & K_{13} & K_{14} & K_{15} & K_{16} \\ K_{21} & K_{22} & K_{23} & K_{24} & K_{25} & K_{26} \\ K_{31} & K_{32} & K_{33} & K_{34} & K_{35} & K_{36} \\ K_{41} & K_{42} & K_{43} & K_{44} & K_{45} & K_{46} \\ K_{51} & K_{52} & K_{53} & K_{54} & K_{55} & K_{56} \\ K_{61} & K_{62} & K_{63} & K_{64} & K_{65} & K_{66} \end{bmatrix}}_{[K]} \underbrace{\begin{Bmatrix} u_{Ax} \\ u_{Ay} \\ \theta_{Az} \\ u_{Bx} \\ u_{By} \\ \theta_{Bz} \end{Bmatrix}}_{\{D\}} \tag{3}$$

Here $\{R\}$ is the reaction forces read from Ansys, $\{K\}$ is the stiffness matrix and $\{D\}$ is the displacement vector. Utilizing unit displacements, the measured reaction forces from Ansys are identical in magnitude to the stiffness entries [12].

However, as the solid elements (SOLID185) are incapable of applying moments or prescribed rotations, remote points are used to apply these.

Remote points are used to approximate the behaviour and kinematics of boundaries and geometries with the use of a single pilot node, which has six degrees of freedom (three translations and three rotations), ultimately allowing to apply rotations and moments. In Figure 7 an example of this can be seen, where MPC equations are used.

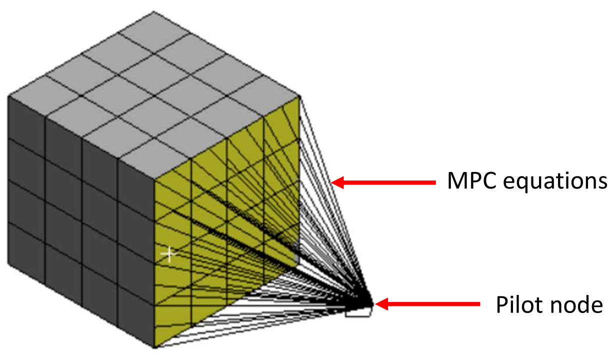


*Fig. 7 Remote point overview, with pilot node and MPC formulations.*

### 3.4 Strength

Strength analysis of the TE core is conducted, to evaluate if the new design is capable of sustaining the loads during operation.

The operation load case is modelled similarly to the buckling case, as the LTT scenario results in the highest strain in the core according to the Student Blade model. However, in this case, it is no longer enough to simply establish a baseline model, as the actual strains and stresses are needed.

Instead, the strains in the Student Blade model are measured, compared to the strains in the 3 [m] sub-model and the ratio between them is found. The loads in the 3 [m] sub-model are scaled with the ratio, such that the strains are similar. This results in a strain distribution deemed comparable with the Student Blade model, while the maximum von Mises strain value is $\varepsilon = 0.008122$ [mm/mm] in both models. The scaled load is then applied to a 3 [m] sub-model with an optimized TE core design, and the resulting stresses are compared.

### 3.5 Optimization

Optimization is utilized to reduce the increase of mass from the change in material to PC. However, PUR material properties are used in the optimization model, as this is the original material. Furthermore, it is isotropic which is computationally efficient in an optimization algorithm, as Ansys utilizes the Solid Isotropic Material with Penalty (SIMP) [14].

Based on the restrictions regarding the shape and size of the TE core, these are unsuited as design variables, and shape/size optimization is eliminated. Thus topology optimization is chosen as the suitable analysis method, where the design variables are the density of each element in a discretized model, ranging from a value of 0 to 1. Here "density" indicates to which degree the element contributes to the objective function.

The used optimization formulation is based on the general formulation from [15] and the goal is to minimize compliance with a specified volume fraction, indicating the amount of material retained.

The compliance is shown to be directly related to the strain energy, $U(\tilde{x}_e)$, resulting in the objective function and adhering constraint equations shown in Equation (4). The outer boundary of the TE core is specified as an exclusion region, meaning the elements are not included in the design space.

$$\begin{aligned} \min_{x} \quad & U(\tilde{x}_e) = \frac{1}{2}\sum_{e=1}^{n} \tilde{x}_e^p \{\mathrm{u}\}^T [\mathrm{k}]_e \{\mathrm{u}\} \\ \text{s.t.} \quad & g(\tilde{x_e}) : \frac{\sum_e v_e \tilde{x}_e}{V^*} - 1 \leq 0 \\ & \tilde{x_e} \in [\varepsilon, 1] \end{aligned} \tag{4}$$

Here $V^*$ is the material resource constraint, $v_e$ is the volume of each element, $[k]_e$ is the element stiffness matrix, $\{u\}$ is the nodal displacement vector and $\tilde{x}_e$ is the filtered element design variable.

Furthermore, $\varepsilon$, which is a small number, is introduced as the lower boundary value of the design variables. This is done to prevent singularities in the stiffness matrix due to a design variable being equal to zero. In Ansys, $\varepsilon$, termed "minimum normalized density" is set to 0.001. Lastly, $p$ is introduced as a penalty term to extremize design variables, i.e. density values close to zero and one are preferred.

The load case used for the optimization is a combination of two load cases given by SGRE, LTT and PTS. Both are considered "Ultimate limit states", meaning worst-case scenarios, and as such, it is deemed unrealistic for both to happen simultaneously. However, the combined case is more representative of the actual load case during operation, and since the TE core should be optimized for a more realistic situation, both are applied.

The LTT load scenario is modelled as described for buckling, where a remote force gives rise to compression in the core. The PTS load case is modelled in a similar manner, with the difference being that the remote point is placed "towards" the SS, i.e. rotating the load from Figure 5 90° clockwise.

The optimization is run with the goal of reaching 3 different volume fractions $V_f = 0.5$, $V_f = 0.3$ and $V_f = 0.15$. However, these were not reached completely due to the program-controlled post-processing in Ansys. The post-processing settings were kept program-controlled, as this would minimize deviation caused by manual input. In Table I the actual percentage of retained material is shown for each design.

| $V_f = 0.5$ | $V_f = 0.3$ | $V_f = 0.15$ |
|---|---|---|
| 57.67% | 40.13% | 27.59% |

*Tab. I Actual % retained mass for each optimization design iteration.*

Each design is exported, extruded to 3 [m] and analysed for the linear buckling and in-plane stiffnesses. In addition, the analyses are performed for the model without any core for comparative purposes.

## 4. Results

The results chosen for assessment of the mechanical performance of the optimized geometries are the buckling load and in-plane stiffnesses. These are plotted in Figures 8 and 9 respectively as a function of the retained mass (volume fraction).

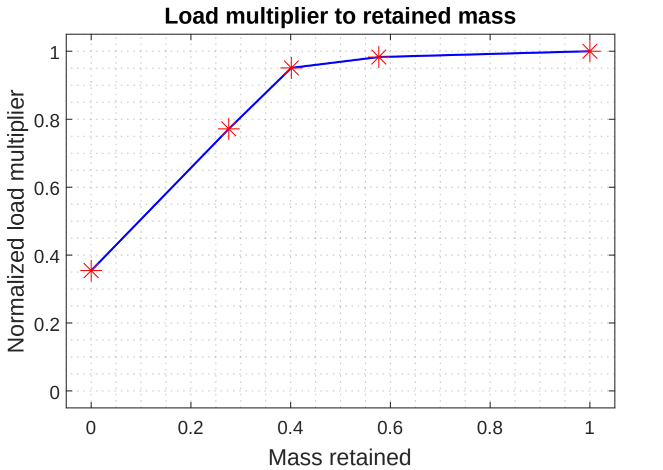


*Fig. 8 Illustration of the relative reduction in mode 1 load multiplier compared to a reduction in mass.*

It is seen that the design with a retained volume of 40%, performs best as it has lost $\approx 5\%$ of buckling resistance. Further removal of material, drastically reduces buckling capabilities.

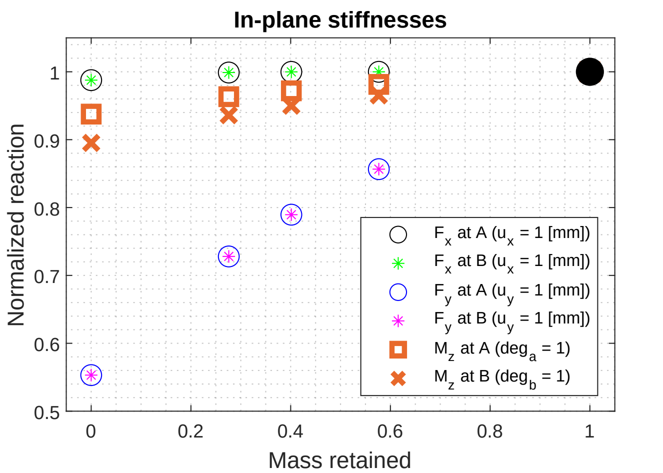


*Fig. 9 Normalized reactions, $k_{ii}$, for different volume fractions.*

The in-plane stiffness analysis reveals the y-direction to be the most sensitive to the reduction of volume. For the same design as highlighted in buckling the reduction of stiffness is $\approx 20\%$

Based on the observations made from the results above, a design is made in order to improve the core. The $V_f = 0.3$ model, shown in Figure 10, is chosen as a base model since this performs best in buckling with the largest amount of material removed.

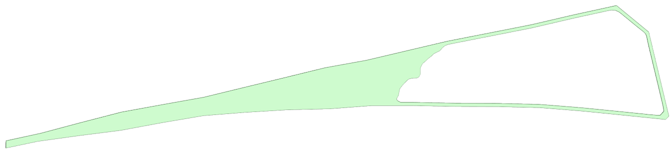

*Fig. 10 Ansys optimized geometry with $V_f = 0.3$.*

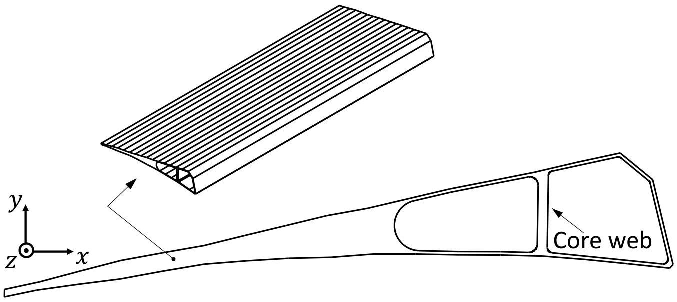


*Fig. 11 The final geometry of the TE core. Based on topology optimization with rough dimensions.*

As seen the optimization results in small amounts of irregularities in material placement along the interface of the removed and retained material.

This is smoothed out with a fillet, the placement and size of which are designed to keep the volume the same. Furthermore, to alleviate the stiffness lost in the y-direction, a "core web" is introduced. The final design is shown in Figure 11.

### 4.1 Comparison

The final design geometry is combined with PC as the material, and the final TE core design is analysed and compared with the original TE core across selected parameters.

Evaluating the mass of the final design is not as simple as just removing 60% of the mass. The selected infill pattern and amount also have a significant influence on the final mass - taking this into account, a total *increase* of mass of 120%, i.e. more than doubling the mass, is achieved. This is a result of a much more dense material, with 40% retained optimized volume and 20% infill with FDM.

With the chosen infill parameters the design can be manufactured in approximately one day. The resulting material parameters are listed in Table II.

| | | |
|---|---|---|
| $E_x$ [GPa] | $E_y$ [GPa] | $E_z$ [GPa] |
| 1.062 | 1.062 | 1.513 |
| $G_{xy}$ [GPa] | $G_{xz}$ [GPa] | $G_{yz}$ [GPa] |
| 0.137 | 0.394 | 0.394 |
| $\nu_{xy}$ | $\nu_{xz}$ | $\nu_{yz}$ |
| 0.157 | 0.252 | 0.252 |
| $\rho = 796.2$ [kg/m$^3$] | | |

*Tab. II PC material properties with 20% grid infill.*

### *4.1.1 Buckling*

The linear buckling load multiplier of the final design with PC is compared with the original load multiplier and it is seen that the new design performs slightly better as the load multiplier increases by $1.5\%$.

To assess the out-of-plane stiffness, a non-linear buckling analysis is conducted. The comparison between the final and original design is shown in Figure 12, plotted as the deflection along a path located at the TE.

It is seen that the deflection, in general, is less pronounced, but still follows the same shape, meaning the extremities are located at the same points but the amplitude is less. From this it is also indicated that the stiffness has been increased, leading to a smaller deflection.

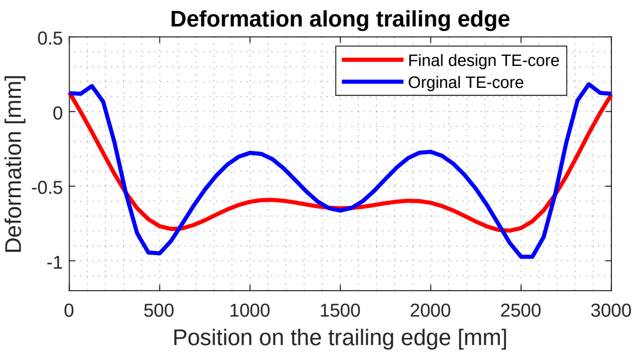


*Fig. 12 Non-linear buckling comparison plotted as deflection along a path located at the edge.*

Furthermore, the maximum out-of-plane deflection is plotted in Figure 13 as a function of the load, yielding a two-dimensional 'load-deflection' curve.

Here it is seen that the two curves are close to identical, with only a few points where the difference is noticeable. At these points, at approximately 1 [mm] and 2 [mm], the force is slightly higher, which indicates higher stiffness.

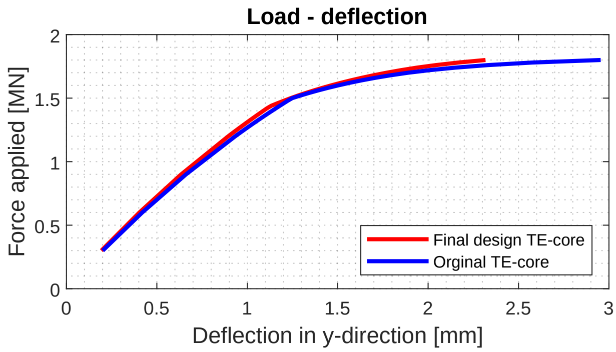


*Fig. 13 Non-linear buckling comparison plotted as force-displacement curve*

### *4.1.2 In-plane stiffnesses*

Equation (5) presents the relative in-plane stiffness results, where the final design made of PC is compared with the original PUR TE core. The entrances indicate the relative difference in %, comparatively with the same entrance in the 6x6 stiffness matrix, i.e. $k_{11}$ sees a $2\%$ increase in the final design compared with the original.

$$[K]_{\%} = \left[\begin{array}{ccc:ccc} \mathbf{2.0} & 0.7 & 0.5 & \mathbf{2.0} & 0.7 & 0.9 \\ 0.7 & -0.9 & -0.2 & 0.7 & -0.9 & -1.0 \\ 0.5 & -0.2 & 0.1 & 0.5 & -0.2 & -1.1 \\ \hdashline \mathbf{2.0} & 0.7 & 0.5 & \mathbf{2.0} & 0.7 & 0.9 \\ 0.7 & -0.9 & -0.2 & 0.7 & -0.9 & -1.0 \\ 0.9 & -1.0 & -1.1 & 0.9 & -1.0 & -0.2 \end{array}\right] \tag{5}$$

It is seen that the properties of the improved geometry with PC material properties behave nearly identically with the original TE core.

There is a slight increase in stiffness in the x-direction of $2\%$, which is most likely due to the change in material, as no specific improvements have been made for the geometry in this direction.

The core web is seen to have been effective in solving the problem with a reduction of stiffness in the y-direction, as these values differ a maximum of $0.9\%$ from the original TE core. The structure has then achieved comparable stiffness, with a $60\%$ reduction in material usage, though with a doubling of mass with PC.

### *4.1.3 Strength evaluation*

The strength of the final design is analyzed in a similar way as described for the original core and the results are compared in terms of the equivalent von Mises stresses for both load cases.

#### *LTT - Operation*

The stress distribution of the original PUR TE core and the final design PC TE core for the operation load case is shown in Figure 14 and 15 respectively.

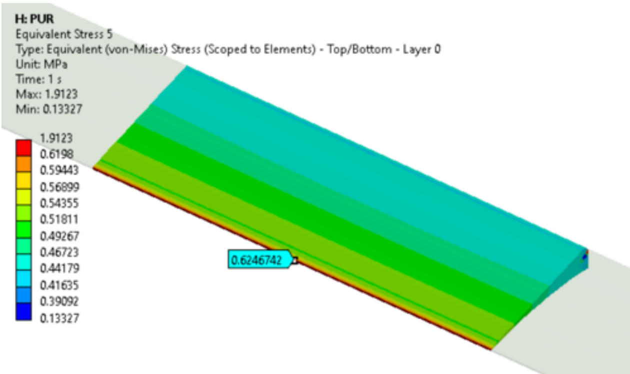


*Fig. 14 Stress distribution of original PUR TE core with operation load case.*

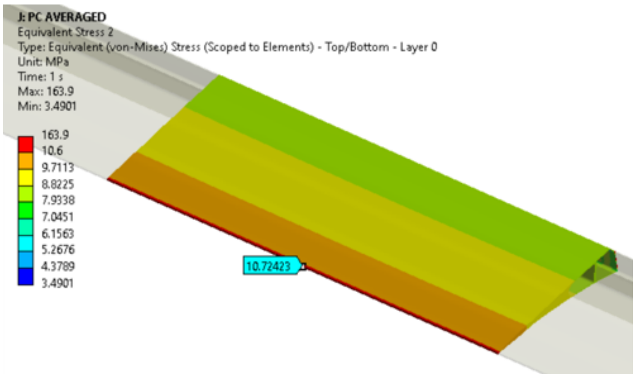


*Fig. 15 Stress distribution of final design PC TE core with operation load case.*

Here it is seen that the equivalent stress is increased significantly from 0.6 [MPa] to 10.7 [MPa] which corresponds to a factor of approximately 18. However, as the ultimate tensile strength of PC is listed as 62 [MPa], the factor of safety is still 5.8 meaning the structure is safe from failure.

It should be noted that stresses above 10.7 [MPa] are present in the model, however, these are due to singularities and as such disregarded. The largest stress is structurally expected to occur in the middle of the model, where the 10.7 [MPa] are measured.

### 4.2 Discussion

#### *4.2.1 Influence of material change versus core web*

It is unclear if the change to a stiffer material or the implementation of the core web has the largest influence on the in-plane stiffnesses. In this section, a discussion based on a parameter investigation is performed.

The investigation aims to separate the influences of the material, by keeping the geometry constant and changing the material from PUR to PC. The influence of the geometry is isolated by keeping the material the same and changing the geometry.

Both investigations are set to be compared to the $V_f = 0.3$, from Figure 10, design with a PUR TE core. This is due to the final design being based on the $V_f = 0.3$ model and as such the geometries vary least along with the volume having comparable values.

Equation (6) shows the relative difference results from influence of geometry investigation. Here the material is kept as PUR, while the geometry is changed.

$$[K]_{\%} = \left[\begin{array}{ccc:ccc} -0.4 & -1.1 & -0.3 & -0.4 & -1.1 & -0.1 \\ -1.1 & \mathbf{5.3} & 2.5 & -1.1 & \mathbf{5.3} & 4.1 \\ -0.3 & 2.5 & 0.5 & -0.3 & 2.5 & 4.7 \\ \hdashline -0.4 & -1.1 & -0.3 & -0.4 & -1.1 & -0.1 \\ -1.1 & \mathbf{5.3} & 2.5 & -1.1 & \mathbf{5.3} & 4.1 \\ -0.1 & 4.1 & 4.7 & -0.1 & 4.1 & 1.0 \end{array}\right] \tag{6}$$

It is seen that the core web has a positive influence on the problematic stiffnesses, specifically the normal direction in y, $k_{22}$, $k_{52}$ and $k_{55}$, and the moment reactions, $k_{32}$, when excited in y. The other values are close to unchanged, meaning the increase is obtained without losing capabilities in other directions.

Equation (7) shows the relative difference results from the influence of material investigation. Here the geometry is kept as $V_f = 0.3$ from Figure 10, while the material is changed.

$$[K]_{\%} = \left[\begin{array}{ccc:ccc} 2.6 & -5.8 & 0.1 & 2.6 & -5.8 & 2.5 \\ -5.8 & \mathbf{20.5} & 10.2 & -5.8 & \mathbf{20.5} & 15.6 \\ 0.1 & 10.2 & 2.5 & 0.1 & 10.2 & 16.7 \\ \hdashline 2.6 & -5.8 & 0.1 & 2.6 & -5.8 & 2.5 \\ -5.8 & \mathbf{20.5} & 10.2 & -5.8 & \mathbf{20.5} & 15.6 \\ 2.5 & 15.6 & 16.7 & 2.5 & 15.6 & 4.2 \end{array}\right] \tag{7}$$

It is immediately noticeable that the material has a major influence on the stiffness properties, as it increases all entrances except for the xy shear stiffness, $k_{12}$.

Especially the stiffness in the y-direction is greatly influenced by the change of material, as seen in the entrances, $k_{i2}$ and $k_{i5}$.

Based on the above, it can be argued that the performance of the final design and material, is influenced more by the material choice than the optimized geometry. However, just changing the material would lead to overly heavy TE cores, which would not be beneficial for production and prototyping.

## 5. Conclusion

A method for producing the TE core using rapid prototyping is presented which shows comparatively similar properties regarding strength, stiffness and buckling behaviour with respect to the original design and material, even though the mass of a single TE core is increased by approximately 120%.

It was found that by utilizing the FDM process the manufacturing time for a single 1 [m] section of the TE core is reduced to around 24 hours. This is a significant reduction in the lead time from design to prototype and will lead to more design freedom.

Thus it is concluded that it is possible to design a specimen for rapid prototyping with the same mechanical behaviour, allowing it to be used for simple testing of new cross-sections and to accelerate new design iterations.

However, it is worth mentioning the possibility of only introducing the optimized TE core geometry to certain sections of the wind turbine blade, i.e. sections which are more prone to failure due to buckling etc. This would reduce the overall increase of mass from introducing an optimized TE core with a denser material in the entire blade.


## Acknowledgement

The authors of this work gratefully acknowledge Grundfos for sponsoring the 10th MechMan symposium.


## References


[1] H. Stiesdal, P. B. Enevoldsen, K. Johansen, J. J. Ö. Kristensen, M. Nörtem, and M. Winther-Jensen, “Method for manufacturing windmill blades. european patent ep1310351a1,” 2003.

[2] P. Liu and G. Chen, Porous Materials. Butterworth-Heinemann, 2014. 978-0-12-407788-1.

[3] S. Kalpakjian and S. R. Schmid, Manufacturing: Engineering AND Technology. Pearson, 2014. 7th edition; ISBN978-981-06-9406-7.

[4] I. Gibson, D. Rosen, B. Stucker, and M. Khorasani, Additive Manufacturing Technologies. Springer, 2021. 3rd edition; ISBN 978-3-030-56126-0.

[5] 3DPrinting.com, 3DPrinting.com, 2022.

[6] all3dp.com, all3dp.com, 2022.

[7] treatstock.co.uk, treatstock.co.uk, 2022.

[8] 3DMaker Engineering, www.3dmakerengineering.com, 2022.

[9] R. Almeida, R. BÃ¶ret, and W. Rimkus, “Simulation of the elastic properties of 3d printed plastic tension rods using fused deposition modeling (fdm),” International Refereed Journal of Engineering and Science, vol. 9, 2020.

[10] Ansys, Material Designer User’s Guide. Ansys, Inc., 2021.

[11] J. Thomsen and R. Pyrz, “The mori tanaka stiffness tensor-diagonal symmetry complex fibre orientations and non-dilute volume fractions,” ELSEVIER, 2001.

[12] R. D. Cook, D. S. Malkus, M. E. Plesha, and R. J. Witt, Concepts AND applications of finite element analysis. John Wiley & Sons, INC., 2001. 4th edition.

[13] F. Lahuerta, N. Koorn, and D. Smissaert, “Wind turbine blade trailing edge failure assessment with sub-component test on static and fatigue load conditions,” 2018.

[14] Ansys, Structural Optimization Analysis. Ansys, Inc., 2021.

[15] J. S. Arora, Introduction to optimum design. Elsevier, 2016. Fourth edition.